Received: 3 September 2018 | Revised: 17 October 2019 | Accepted: 24 October 2019

DOI: 10.1002/jemt.23410

RESEARCH ARTICLE

MICROSCOPY RESEARCH & TECHNIQUE WILEY

Potential of a sensitive uric acid biosensor fabricated using hydroxyapatite nanowire/reduced graphene oxide/gold nanoparticle

Yao Chen[1] | Wencui Zhou[1] | Jiahui Ma[1] | Feixia Ruan[1] | Xuezhen Qi[2] | Yurong Cai[1]

[1]The Key Laboratory of Advanced Textile Materials and Manufacturing Technology of Ministry of Education, National Engineering Lab for Textile Fiber Materials and Processing Technology, School of Materials Science and Engineering, Zhejiang Sci-Tech University, Hangzhou, China

[2]School of Chemistry and Chemical Engineering, Liaocheng University, Liaocheng, China

Correspondence
Yurong Cai, The Key Laboratory of Advanced Textile Materials and Manufacturing Technology of Ministry of Education, National Engineering Lab for Textile Fiber Materials and Processing Technology, School of Materials Science and Engineering, Zhejiang Sci-Tech University, Hangzhou 310018 China.
Email: caiyr@zstu.edu.cn

Funding information
Zhejiang Sci-Tech University, Grant/Award Number: 2019Y006; National Innovation and Entrepreneurship Training Program for College Student, Grant/Award Number: 201810338041

Review Editor: Chuanbin Mao

Abstract

In this study, a ternary nanocomposite consisting of gold nanoparticles (AuNPs), hydroxyapatite (HAP) nanowires, and reduced graphene oxide (rGO) is synthesized by a simple one-step hydrothermal method, which is used to modify glassy carbon electrode (GCE) for detecting uric acid. The nanocomposite is characterized through various methods such as scanning electron microscopy, transmission electron microscopy, and X-ray diffraction. Electrochemical measurements of the modified GCE are performed in a conventional three-electrode system. Experimental results show that the obtained HAP nanowire and rGO are mixed homogeneously, and the AuNPs are deposited into this matrix. The GCE modified by the nanocomposites have superior electrocatalytic activities for uric acid. The peak current intensities of UAO (uricase)/HAP-rGO/AuNPs sensing system linearly increase as the uric acid concentration increases substantially in a range of 1.95×10^{-5} to 6.0×10^{-3} M (R^2 = .9943), with a detection limit of 3.9×10^{-6} M (S/N = 3) and analytical sensitivity of 13.86 mA/M. The biosensor performs well in determining uric acid concentration in human urine samples.

KEYWORDS

biosensor, gold nanoparticles, hydroxyapatite, reduced graphene oxide, uric acid

1 | INTRODUCTION

Uric acid (UA) is an end product of purine metabolism in our human body (Akyilmaz, Sezgintürk, & Dinçkaya, 2003). It is generated by enzymatic reactions including xanthine oxidase. The normal level of UA in human urine is between 0.13 and 0.46 mM, which changes when a person is suffering from some diseases such as hyperuricemia, chronic renal diseases, cardiovascular diseases, and so forth (Alwahsh & Gebhardt, 2016; Becker & Jolly, 2006; Huang et al., 2004). The understanding of UA concentration in human urine or serum is vital in clinical analysis and diagnosis through a rapid, easy, and inexpensive method is urgent. The conventional test methods for UA concentration include chemical methods, spectrophotometry, enzymatic-colorimetric method (Hall, 2008), electroanalysis (Sun, Lee, Yang, & Wu, 2011), chromatography (Ensafi & Karimi-Maleh, 2010), and fluorimetry (Arora, Nandwani, Bhambi, & Pundir, 2009). Some shortcomings of these methods, such as expensive, complex, and unbefitting for real clinical analysis (Da Costa et al., 2016), are undeniable. By contrast, electrochemical biosensor is an attractive alternative due to its simplicity, low cost, excellent selectivity, and high sensitivity (Wang, Gao, Sun, & Xu, 2014; Xu, Liu, Su, Liu, & Qiu, 2011; Zhao, Yu, Tian, & Xu, 2016). Electrochemical applications of biosensors such as uric acid biosensors based on enzyme catalytic reactions are reported in the documents (Brusova, Ferapontova, Sakharov, Magner, & Gorton, 2005; Dai, Bao, & Yang, 2008; Dung, Patil, & Duong,

Yao Chen and Wencui Zhou contributed equally to this study and share first authorship.

2012; Shimomura, Itoh, & Sumiya, 2008). For instance, Muhamad Nadzmi Omar made a electrochemical biosensor to detect uric acid, and the uric acid electrochemical biosensor has a wide working range of 0.02–0.49 mM and low detection limit 3.45 μM, which is better than other methods (Omar, Salleh, Lim, & Tajudin, 2016).

Calcium phosphate salts are a class of inorganic materials with great application potential in the fields of pharmaceutical carriers, implant materials, adsorbents due to their excellent biocompatibility and strong adsorption property (Wu, Liu, Cai, & Yao, 2013), especially hydroxyapatite (HAP). Recently, some HAP-related biosensors have been developed to detect glucose and luteolin (Bharath et al., 2015; Pang, Liu, Zhang, Gao, & Hu, 2014). Frequently, carbon nanotube and graphene have been added into the biosensors to enhance conductivity of the electrode (Ghanbari & Moloudi, 2016; Guo et al., 2010; Jia, Delgado, Terrones, Meunier, & Dresselhaus, 2011; Teymourian, Salimi, Firoozi, Korani, & Soltanian, 2014; Wang, Shen, Yao, & Park, 2009). Graphene, a novel carbon material, has broad prospects in fields of sensors and energy storage due to its large specific surface area, strong adsorption, good electrical conductivity, and high strength. For example, a reduced graphene oxide (rGO) modified electrode has been used to systematically study the electrochemical signals such as DNA and enzyme by Zhou, Zhai, and Dong (2009) and an improved properties has been obtained.

In the study, the composite of HAP nanowires and rGO (HAP/rGO) is fabricated through a simple one-step method. Gold nanoparticles (AuNPs) are included due to its excellent catalytic activity and signal amplifying function (He et al., 2016). The uricase (UAO)-loaded HAP-rGO/AuNPs composites are used to modify glassy carbon electrode (GCE) for uric acid detection. Schematic diagram of HAP-rGO/AuNPs/GCE sensing system is presented in Scheme 1. The HAP-rGO/AuNPs biosensor shows excellent sensitivity, wide linearity range, and high selectivity for uric acid detection.

2 | MATERIALS AND METHODS

2.1 | Reagents and apparatus

Uricase (UAO) (EC232-655-5, 19.7 U/mg) from Arthrobacter globiformis and uric acid with 99% purity were obtained from Sigma. All other chemicals were purchased from Hangzhou Mike Chemical Agents Company, China. Chloroauric acid ($HAuCl_4{\cdot}4H_2O$) was purchased from traditional Chinese medicine. All reagents were analytical grade and directly used without further purification. Both Na_2HPO_4 (99% purity) and NaH_2PO_4 (99% purity) were used to prepare phosphate buffer solution (PBS). In all experiments, ultrapure water was used.

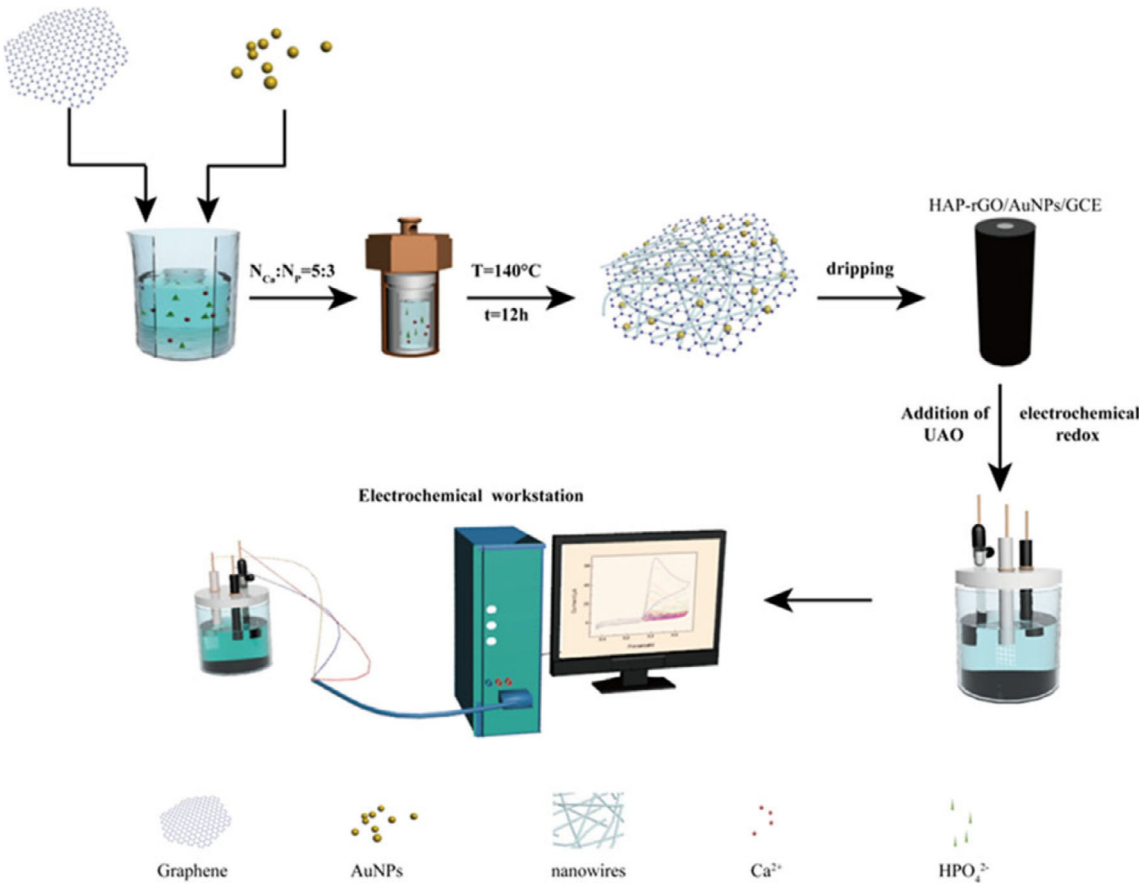

SCHEME 1 Schematic illustration of the preparation and application of HAP-rGO/AuNPs/GCE sensing system. AuNP, gold nanoparticle; GCE, glassy carbon electrode; HAP, hydroxyapatite; rGO, reduced graphene oxide [Color figure can be viewed at wileyonlinelibrary.com]

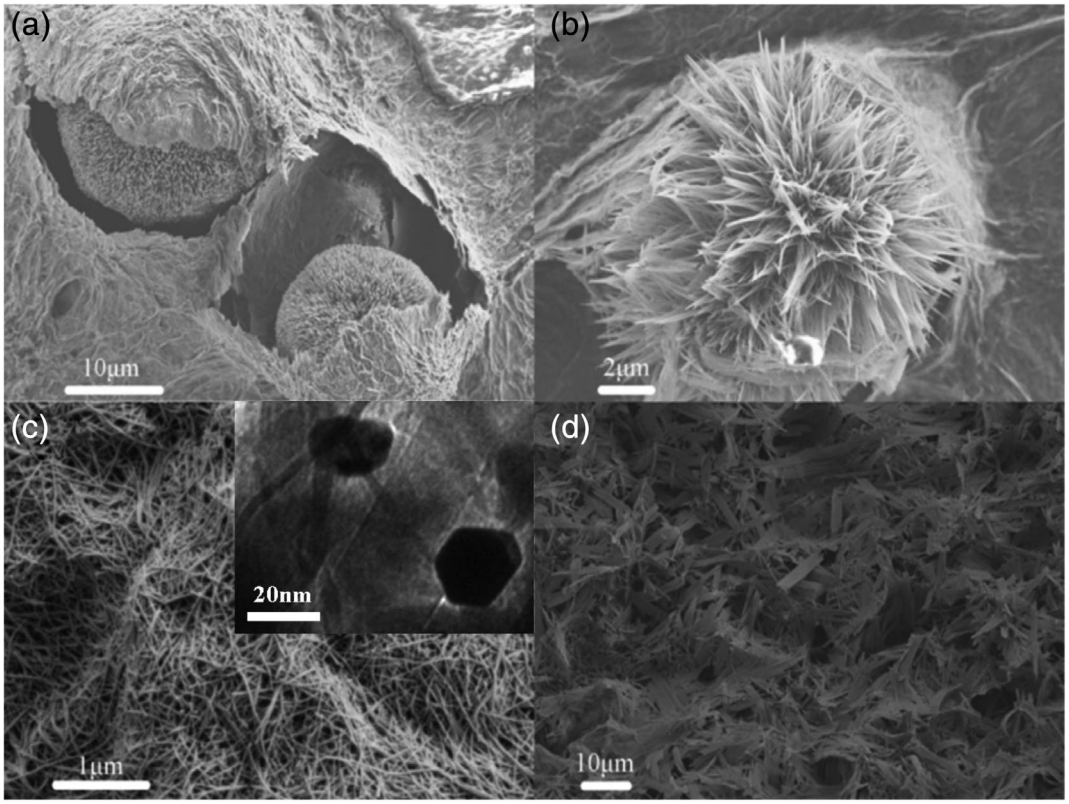

FIGURE 1 SEM images of the HAP-rGO/AuNPs nanocomposite prepared at different pH values: (a) 3.5, (b) 4, (c) 4.5, and (d) 5.5. The inserted image in the right-top corner of (c) is its TEM image. AuNP, gold nanoparticle; HAP, hydroxyapatite; rGO, reduced graphene oxide; SEM, scanning electron microscopy; TEM, transmission electron microscopy

Morphology of the fabricated composite was observed using scanning electron microscopy (FE-SEM, Hitachi S-4800) and transmission electron microscopy (TEM, JEM-1230) measurements. X-ray powder diffraction (XRD, ARL X'TRA, Switzerland) was performed using Cu Kα irradiation with a scan range of 10–60°. The X-ray source was operated at 40 kV and 40 mA. Electrochemical properties of samples were measured using a CHI 660D workstation (Shanghai Chenhua, China) with a traditional three-electrode system. The working electrode was the modified GCE. Nitrogen is pumped into buffers for at least 30 min to purge the solution, and subsequent electrochemical measurements were performed under nitrogen atmosphere at room temperature.

2.2 | Synthesis and characterization of citrate-stabilized AuNPs

Au nanoparticles were synthesized by the following method. Chloroauric acid (1 g) was dissolved in 100 ml of ultrapure water. Then 1 ml of the above solution was diluted by 99 ml ultrapure water in a 250 ml round-bottom flask and then was heated to boiling. Two milliliters of sodium citrate solution (10 g/L) was added to the above flask under vigorous stirring, which induced a color change of Au chloride solution from yellow to purple. The change indicated the formation of Au clusters. The mixture solution was boiled for another 15 min and then cooled to room temperature under continuous stirring to obtain the AuNPs solution (Masitas, Allen, & Zamborini, 2016). The final AuNPs was characterized by TEM and UV. UV–VIS was measured at room temperature and the absorption peak was at around 520 nm.

2.3 | Synthesis and characterization of HAP-rGO/AuNPs

First, a total of 60 mM Na_2HPO_4 and 100 mM $CaCl_2$ solutions were precooled at 15°C for 1 hr. The two solutions were then mixed with the same volume, and the Ca and P ratio was kept at 1.67 (Li et al., 2016). Next, 5 ml GO synthesized by a modified Hummers method and 5 ml AuNPs prepared by above-mentioned procedure were added to the mixture under continuously stirring. The pH of the mixture solution was rapidly adjusted to 4.5 using 0.1 M hydrochloric acid. After precooling at 15°C for another 1 hr, the mixture was then dumped into a Teflon-lined stainless steel autoclave and dwelled at 140°C for 12 hr. Finally, the product was separated by vacuum filtration and washed three times by ultrapure water. The product was then dried at 60°C.

2.4 | Fabrication of UAO/HAP-rGO/AuNPs biosensor

Glassy carbon electrode was polished first using alumina slurry to reach a shiny finish and then was rinsed thoroughly by ultrapure water and ethanol under ultrasonic condition. And then the electrode was further treated by multicycle voltammetry from −1.0 to 1.0 V in 0.5 M H_2SO_4 aqueous solution at a scan rate of 50 mV/s. Lastly, the electrode was rinsed thoroughly with ultrapure water and dried at room temperature (Li, Li, Liu, Zhang, & Chen, 2017).

A 50 mg/ml homogeneous mixture was prepared by adding 100 mg of the prepared HAP-rGO/AuNPs composite in 2 ml of ultrapure water by sonication for 1 min. The prepared homogeneous solution was dropped onto the surface of the treated GCE by a 10 μl pipette and dried in an oven at 60°C. This process was performed three times. Finally, the uricase solution was dropped on the GCE to obtain the UAO/HAP-rGO/AuNPs working electrode. This process was repeated for two times.

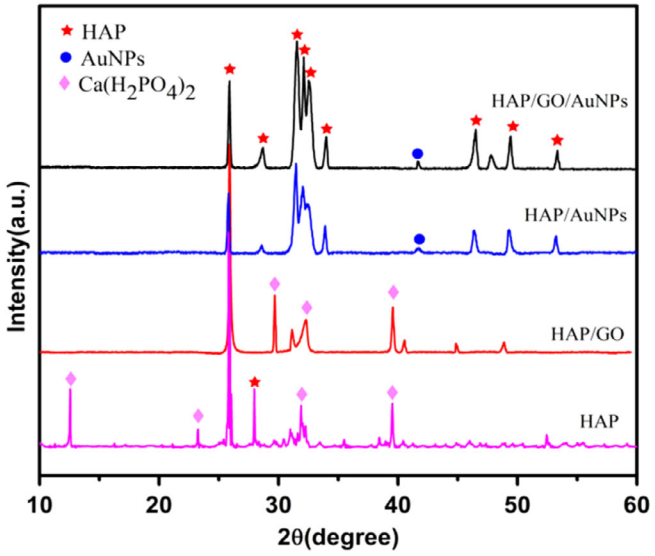

FIGURE 2 XRD patterns of HAP, HAP/GO, HAP/AuNPs and HAP/rGO/AuNPs. AuNP, gold nanoparticle; HAP, hydroxyapatite; rGO, reduced graphene oxide; XRD, X-ray diffraction [Color figure can be viewed at wileyonlinelibrary.com]

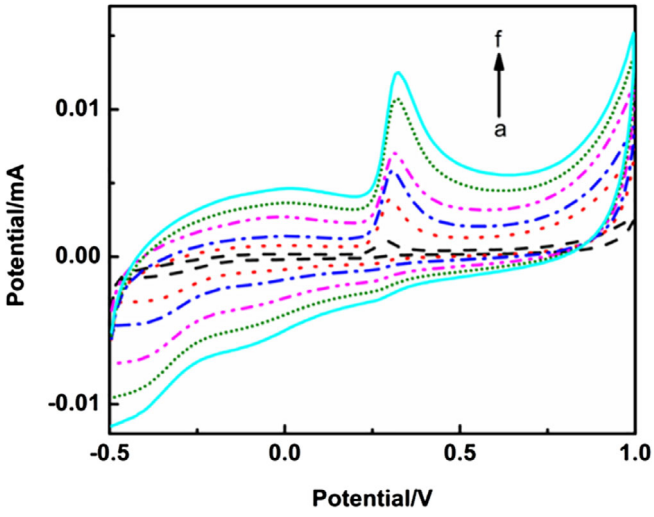

FIGURE 4 Cyclic voltammograms of UAO/HAP-rGO/AuNPs/GCE in presence of 2×10^{-4} mol L^{-1} uric acid in PBS (pH 7.0) with different scan rates (a → f): 0.001, 0.005, 0.01, 0.02, 0.03, and 0.04 Vs^{-1}, respectively. AuNP, gold nanoparticle; GCE, glassy carbon electrode; HAP, hydroxyapatite; PBS, phosphate buffer solution; rGO, reduced graphene oxide [Color figure can be viewed at wileyonlinelibrary.com]

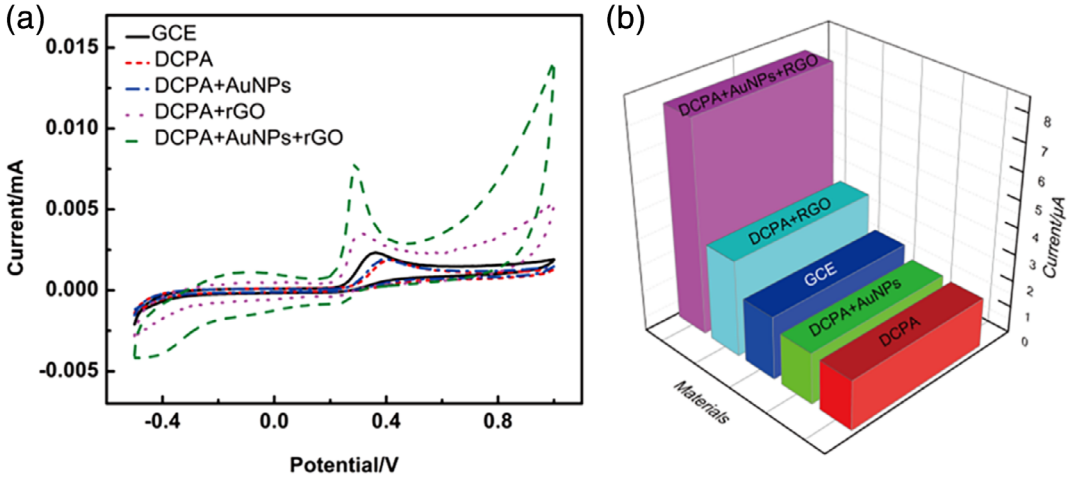

FIGURE 3 (a) CV of the bare GCE electrode and the modified GCE electrode by HAP, HAP/AuNPs, HAP/rGO, HAP-rGO/AuNPs, respectively. (b) The histogram of current response of GCE modified by different composite materials. Measurements in 0.2 mM uric acid solution, scan rate: 50 mV/s. AuNP, gold nanoparticle; CV, cyclic voltammetry; GCE, glassy carbon electrode; HAP, hydroxyapatite; rGO, reduced graphene oxide [Color figure can be viewed at wileyonlinelibrary.com]

3 | RESULTS AND DISCUSSION

3.1 | Characterization of the electrode materials

The effect of solution pH values on the morphology of HAP-rGO/AuNPs is investigated using SEM and TEM at constant reaction temperature of 140°C and reaction time of 12 hr (Figure 1). The spherical HAP particles can be fabricated when pH is 3.5 (Figure 1a). HAP spheres are encapsulated by rGO layers. The shape of HAP changes into a thorn ball when pH increases to 4.0 and rGO uniformly envelope the HAP balls (Figure 1b). As pH is 4.5, HAP nanowires are formed (Figure 1c). The nanowires are homogeneous and dispersed. The diameter of these nanowires is about 10–15 nm. TEM image of the sample inserted in the right-top corner of Figure 1c shows that the AuNPs are uniformly scattered in the HAP/rGO composite materials. The size of AuNPs is about 20 nm. The width of the HAP nanowires increases to about 2.5 μm with the increase of pH from 4.5 to 5.5 (Figure 1d). In subsequent experiments, HAP nanowire fabricated at pH 4.5 is chosen as the substrate material due to its large specific surface area and better film forming ability.

X-ray diffraction is used to analyze the chemical composition of the samples as-prepared at pH 4.5 and 140°C (Figure 2). Several peaks in the patterns of HAP and HAP/GO samples correspond to $Ca(H_2PO_4)_2$ (JCPDS 09-0390) and HAP (JCPDS 09-0432), respectively. In patterns of HAP/AuNPs and HAP/ GO/AuNPs, the peak at 41.603° ascribed to AuNPs (JCPDS 26-1006) indicates that AuNPs are blended in the composites. Compared with HAP and HAP/GO samples, more HAP characteristic peaks are observed in patterns of HAP/AuNPs and HAP/GO/AuNPs, which imply that the addition of gold particles influences the reaction environment and cause a phase transition from $Ca(H_2PO_4)_2$ to HAP. No obvious peaks of rGO are detected in the patterns due to the limit content of rGO in the composites.

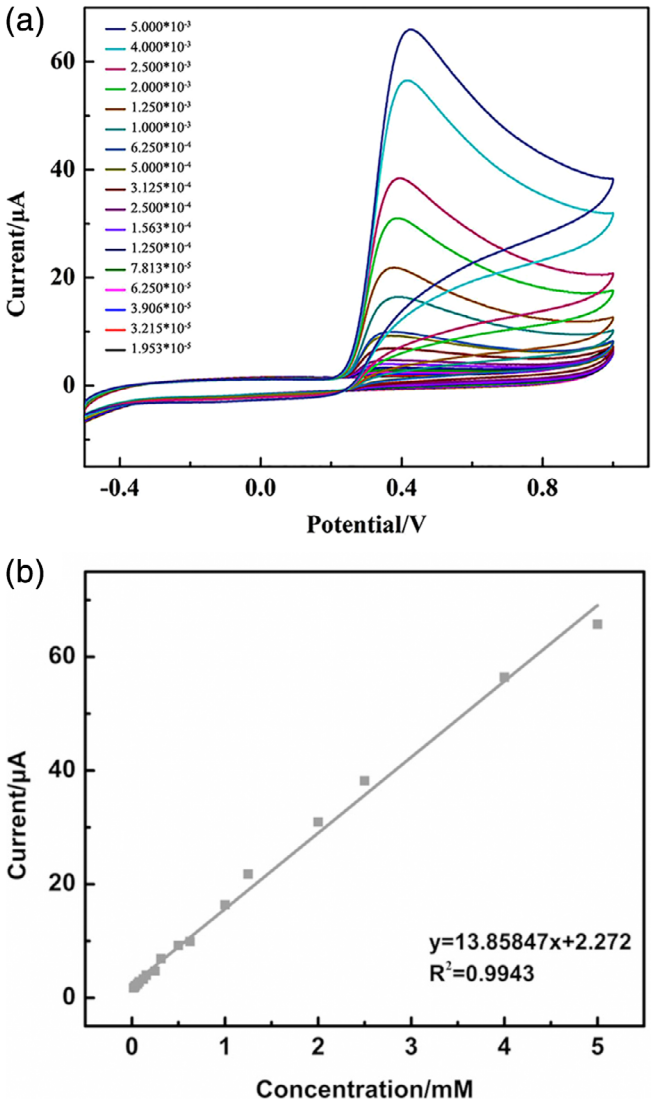

FIGURE 5 (a) CV curves of UAO/HAP-rGO/AuNPs/GCE sensing system in 0.1 M PBS (pH 7.0) after the addition of uric acid. Uric acid concentration increases from 1.953×10^{-5} to 3.215×10^{-5}, 3.906×10^{-5}, 6.250×10^{-5}, 7.813×10^{-5}, 1.250×10^{-4}, 1.563×10^{-4}, 2.500×10^{-4}, 3.125×10^{-4}, 5.000×10^{-4}, 6.250×10^{-4}, 1.000×10^{-3}, 1.250×10^{-3}, 2.000×10^{-3}, 2.500×10^{-3}, 4.000×10^{-3} to 5.000×10^{-3} M, respectively. (b) Linear relationship between the current peak intensity (I_p) of UAO/HAP-rGO/AuNPs/GCE and the uric acid concentration. AuNP, gold nanoparticle; CV, cyclic voltammetry; GCE, glassy carbon electrode; HAP, hydroxyapatite; PBS, phosphate buffer solution; rGO, reduced graphene oxide [Color figure can be viewed at wileyonlinelibrary.com]

3.2 | Direct electrochemistry of HAP-rGO/AuNPs modified electrodes

Cyclic voltammetry (CV) is a common and useful technique for investigating the direct electrochemistry of UAO on HAP-RGO/AuNPs

TABLE 1 Performance comparison of the uric acid biosensors between references and in this work

Electrodes	Linear range (mM)	LOD (μm)	References
Fc-GO/SPE	0.001–0.02	0.1	Dey and Raj (2013)
PC/UOx/CA/CoPC/SPCE	0.015–0.25	15	Kanyong, Pemberton, Jackson, and Hart (2012)
UAO/GO	0.02–0.49	3.45	Omar et al. (2016)
CuO nanorods/graphite	0.004–0.8	4	Wang et al. (2010)
PBNPs/c-MWCNT/PANI	0.005–0.8	5	Rawal, Chawla, Chauhan, Dahiya, and Pundir (2012)
AuNPs/MWCNT	0.01–0.8	0.01	Chauhan and Pundir (2011)
UAO/HAP-rGO/AuNPs	0.0195–5.0	3.9	This work

Abbreviations: AuNP, gold nanoparticle; HAP, hydroxyapatite; rGO, reduced graphene oxide.

modified electrodes. Uricase (UAO) is selected as a typical enzyme for research the application of HAP-rGO/AuNPs nanostructures for biosensing because of its prominent role in UA monitoring. The direct electrochemistry of UAO-immobilized HAP-rGO/AuNPs modified electrode has been examined in N_2-saturated PBS (pH 7) with a scan rate of 50 mV/s. Figure 3a shows the cyclic voltammograms of GCE-, HAP-, HAP/AuNPs-, HAP/rGO-, and HAP-rGO/AuNPs modified GCE in PBS (pH 7) at a scan rate of 50 mV/s. The GCE shows featureless redox peaks within the potential range of −0.5 to 1.0 V. Curves of HAP and HAP/AuNPs present a negligible redox peak current. Furthermore, a well-defined redox peak is observed in the HAP-rGO/AuNPs modified GCE. The CV curve for HAP-rGO/AuNPs modified GCE is apparently larger than those of the pure HAP and HAP/rGO modified GCE (Figure 3b). Moreover, the HAP-rGO/AuNPs modified GCE shows a well-defined redox peak, which indicates the favorable direct electron transfer of UA on the electrode.

The cyclic voltammograms of UAO/HAP-rGO/AuNPs/GCE at various scan rates are measured (Figure 4). The result illustrates the cyclic voltammograms of UAO/HAP-rGO/AuNPs/GCE obtained in the range of 0.001–0.04 V/s in PBS buffer (pH 7.0) containing 2×10^{-4} mol L^{-1} UA. It also shows that the redox peak value increase with the increase of scan rates. The immobilization of UA at the surface of the UAO/HAP-rGO/AuNPs/GCE can be attributed to the notorious adsorption of HAP. The results suggest that the UAO/HAP-rGO/AuNPs/GCE provides rapid electron transfer between the redox center of the UA and the surface of UAO/HAP-rGO/AuNP composite.

Figure 5a shows the typical cyclic voltammogram curves at different UA concentrations and peak currents increase regularly with the increase of UA concentration from 0 to 5 M. As shown in Figure 5b, the increase of the reduction current is linear in the range of 0.0195 to 5 mM, and the linear regression equation is fitted to

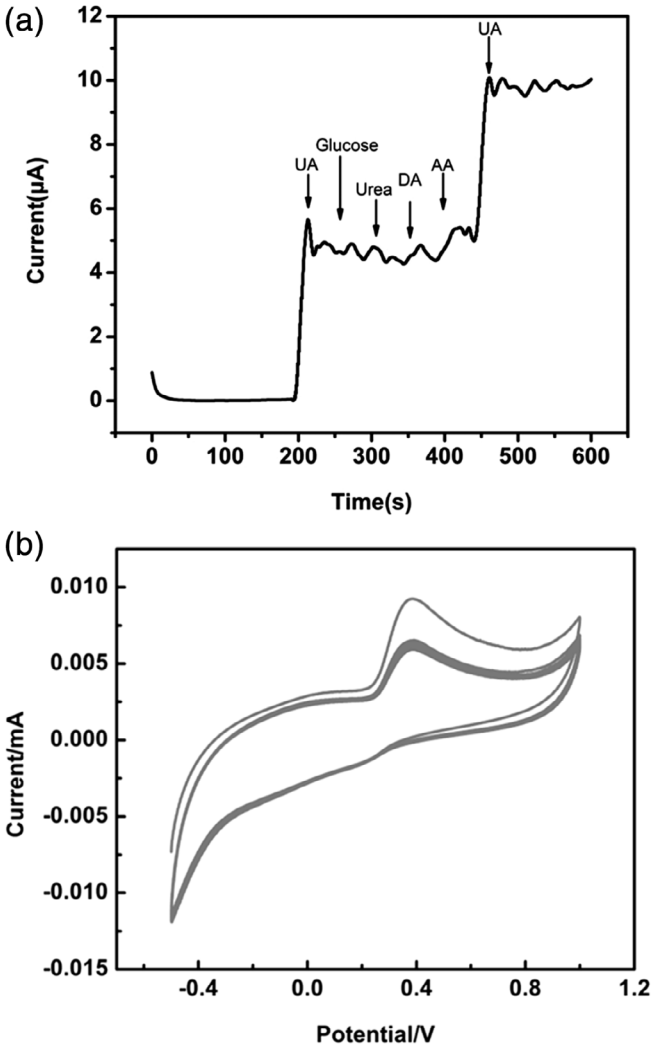

FIGURE 6 (a) Selectivity profile of electrode over interfering species of glucose, urea, DA, and AA; (b) Repetitive cyclic voltammograms of UAO/HAP-rGO/AuNPs/GCE taken out in the presence of 0.2 mM uric acid in PBS (pH 7.0) with 20 cyclic numbers. Scan rate: 50 mV s^{-1}. AuNP, gold nanoparticle; GCE, glassy carbon electrode; HAP, hydroxyapatite; PBS, phosphate buffer solution; rGO, reduced graphene oxide

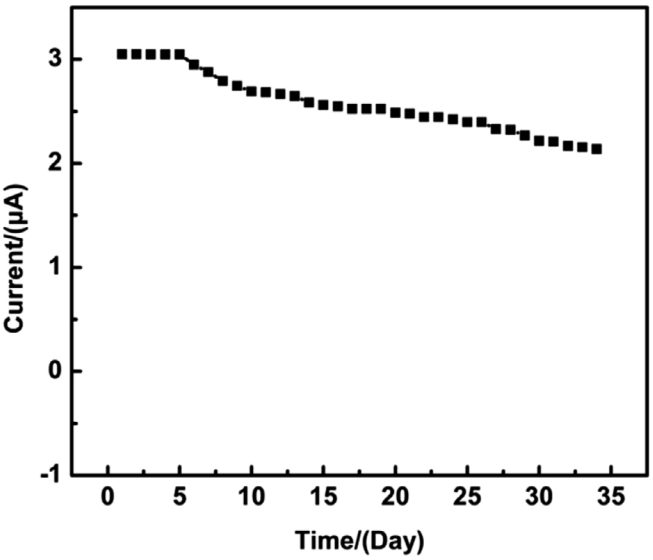

FIGURE 7 Effect of storage time on the response of UAO/HAP-rGO/AuNPs/GCE electrodes. AuNP, gold nanoparticle; GCE, glassy carbon electrode; HAP, hydroxyapatite; rGO, reduced graphene oxide

TABLE 2 Comparison of the measured UA content to the theoretical UA content

No.	Added UA content (mmol)	Measured UA content (mmol)	Percentage of measured UA content to theoretical UA content (%)	Average percentage (%)
1	0	0.583	–	99.12
2	0.2	0.785	100.26	
3	0.4	0.971	98.78	
4	0.6	1.163	98.31	

Abbreviation: UA, uric acid.

$$i_{pa} = 13.85847C + 2.272 \left(R^2 = .9943, n = 3\right).$$

The sensitivity of the biosensor is 13.86 μAm M^{-1}, and the detection limit (LOD) is 3.9×10^{-6} mol L^{-1} at a signal-to-noise ratio of 3. The low LOD may be due to the higher load content of UAO ascribed to the large surface area, strong adsorption of HAP nanowires, good electroconductivity of rGO and excellent catalytic activity of AuNPs in UAO/HAP-rGO/AuNP/GCE. The UAO/HAP-rGO/AuNPs/GCE indicates superior performance compared with most of the previously reported systems (Table 1), especially in linear range.

3.3 | Application performance of HAP-rGO/AuNPs modified electrodes

Natural blood and urine are mixtures and there are a lot of chemicals in them, which probably interferes the amperometric detection of UA. The selectivity of a UA sensor depends on two factors: the enzyme–analyte reaction and the selective mechanism. The enzyme–analyte reaction is specific with respect to the nature of the uricase functionality, that is, it only reacts with UA. The possible interferences in blood includes AA, urea, DA, and glucose. The anti-interference measurement of the UA sensor is carried out in the presence of ascorbic acid (AA), urea, dopamine (DA), and glucose (Figure 6a). An amperometric *i*–*t* curve is recorded using a fixed concentration of UA (0.2 mM) and varying concentrations of glucose (5 mM), urea (0.2 mM), DA (0.1 mM), and AA (0.1 mM) added in the PBS following a certain order. No evident current change is observed after the addition of interfering agents. Only AA induces a slight fluctuation of current, but such fluctuation was not evident. The results indicate that the obtained sensor can selectively detect the UA and offers credible signal when the interfering species reach high concentrations. The anti-interference ability of the modified UA sensor can be ascribed to the enzyme–analyte reaction and the selective mechanism between uricase and UA. To determine the repeatability of UAO/HAP-rGO/AuNPs/GCE, four intermittent determinations of a UA solution (2×10^{-4} M) are performed, where obtained relative standard deviation (RSD) is 2.4%. The stability of the UAO/HAP-rGO/AuNPs/GCE is carried out by continuous scanning for 20 cycles from −0.5 to 1.0 V in PBS solution (pH 7) containing 2×10^{-4} M UA. The anodic peak current descends gradually with cyclic time increasing and tends to be stable after three cycles (Figure 6b).

To evaluate the stability of UAO/HAP-rGO/AuNPs/GCE, the electrode is dwelled at 4°C for 35 days and its current response ability is measured every day during these periods. As shown in Figure 7, a slow current decrease appears with the increase of the dwelling time. Compared with the original current, 30% decay of current is obtained after 35 days storage. Furthermore, four UAO/HAP-rGO/AuNPs/GCE electrodes are fabricated using the same method to determine the stability of the preparation process. The stability of electrodes is measured through the DPV method. The RSD among different electrodes is less than 4% and no significant difference is observed in current responses, which suggests that UAO/HAP-rGO/AuNPs/GCE electrode has good reproducibility.

The UA content in human urine is detected using the modified UAO/HAP-rGO/AuNPs/GCE to evaluate its practicality by standard addition method, which is 0.583 mmol in 1 L urine. Subsequently, 0.2, 0.4, 0.6 mmol UA are added in the human urine, respectively. UA concentration is measured using the modified GCE again. The results are shown in Table 2. The percentage of measured UA content to theoretical UA content ranges from 98.31 to 100.26% with the increase of UA concentration from 0.583 to 1.183 mM. The average percentage is 99.12%, indicating a higher accuracy of the sensor. The results confirm that the UAO/HAP-rGO/AuNPs electrode is suitable for the sensitive detection of UA level in human urine with a rapid speed.

4 | CONCLUSIONS

This work proposes a relatively simple uricase biosensor consisting of uricase/HAP-rGO/Au nanoparticles/GCE (UAO/HAP-rGO/AuNPs/GCE). The synergism of components awards the electrode a favorable biocompatibility, strong adsorption for uricase, rapid electron transfer ability of UA, and subsequent excellent electrochemical properties, including high sensitivity, low detection limit, rapid current response speed, and large linear calibration range. In addition, the electrode holds high storage stability and reproducibility in preparation process. We believe that the job has developed a potential approach for rapid and accurate investigation of UA in clinical.

ACKNOWLEDGMENTS

This research work was financially supported by National Innovation and Entrepreneurship Training Program for College Student (201810338041) and the Fundamental Research Funds of Zhejiang Sci-Tech University (2019Y006).

ORCID

Yurong Cai https://orcid.org/0000-0003-1942-8931

REFERENCES

Akyilmaz, E., Sezgintürk, M. K., & Dinçkaya, E. (2003). A biosensor based on urate oxidase–peroxidase coupled enzyme system for uric acid determination in urine. *Talanta*, *61*, 73–79.

Becker, M. A., & Jolly, M. (2006). Hyperuricemia and associated diseases. *Rheumatic Disease Clinics of North America*, *32*, 275–293.

Huang, S. H., Shih, Y. C., Wu, C. Y., Yuan, C. J., Yang, Y. S., Li, Y. K., & Wu, T. K. (2004). Detection of serum uric acid using the optical polymeric enzyme biochip system. *Biosensors and Bioelectronics*, *19*, 1627–1633.

Alwahsh, S. M., & Gebhardt, R. (2016). Dietary fructose as a risk factor for non-alcoholic fatty liver disease (NAFLD). *Archives of Toxicology*, *91*(4), 1545–1563.

Hall, M. B. (2008). Determination of starch, including maltooligosaccharides, in animal feeds: Comparison of methods and a method recommended for AOAC collaborative study. *Journal of AOAC International*, *92*(1), 42–49.

Sun, C. L., Lee, H. H., Yang, J. M., & Wu, C. C. (2011). The simultaneous electrochemical detection of ascorbic acid, dopamine, and uric acid

using graphene/size-selected Pt nanocomposites. *Biosensors and Bioelectronics*, *26*, 3450–3455.

Ensafi, A. A., & Karimi-Maleh, H. (2010). Modified multiwall carbon nanotubes paste electrode as a sensor for simultaneous determination of 6-thioguanine and folic acid using ferrocenedicarboxylic acid as a mediator. *Journal of Electroanalytical Chemistry*, *640*(1), 75–83.

Arora, J., Nandwani, S., Bhambi, M., & Pundir, C. S. (2009). Fabrication of dissolved O_2 metric uric acid biosensor using uricase epoxy resin biocomposite membrane. *Analytica Chimica Acta*, *647*, 195–201.

Da Costa, E. T., Santos, M. F., Jiao, H., do Lago, C. L., Gutz, I. G., & Garcia, C. D. (2016). Fast production of microfluidic devices by CO_2 laser engraving of wax-coated glass slides. *Electrophoresis*, *37*(12), 1691–1695.

Xu, C., Liu, Y., Su, F., Liu, A., & Qiu, H. (2011). Nanoporous PtAg and PtCu alloys with hollow ligaments for enhanced electrocatalysis and glucose biosensing. *Biosensors and Bioelectronics*, *27*, 160–166.

Wang, J., Gao, H., Sun, F., & Xu, C. (2014). Nanoporous PtAu alloy as an electrochemical sensor for glucose and hydrogen peroxide. *Sensors and Actuators B: Chemical*, *191*, 612–618.

Zhao, D., Yu, G., Tian, K., & Xu, C. (2016). A highly sensitive and stable electrochemical sensor for simultaneous detection towards ascorbic acid, dopamine, and uricacid based on the hierarchical nanoporous PtTi alloy. *Biosensors and Bioelectronics*, *82*, 119–126.

Shimomura, T., Itoh, T., & Sumiya, T. (2008). Electrochemical biosensor for the detection of formaldehyde based on enzyme immobilization in mesoporous silica materials. *Sensors & Actuators B: Chemical*, *135*, 268–275.

Dung, N. Q., Patil, D., & Duong, T. (2012). Amperometric glucose biosensor based on a GOx-entrapped TiO_2-SWCNT composite. *Sensors & Actuators B: Chemical*, *103*, 166–167.

Dai, Z., Bao, J., & Yang, X. (2008). A bienzyme channeling glucose sensor with a wide concentration range based on co-entrapment of enzymes in SBA-15 mesopores. *Biosensors & Bioelectronics*, *23*, 1070–1076.

Brusova, Z., Ferapontova, E. E., Sakharov, I. Y., Magner, E., & Gorton, L. (2005). Bioelectrocatalysis of plant peroxidases immobilized on graphite in aqueous and mixed solvent media. *Electroanalysis*, *17*, 460–468.

Omar, M. N., Salleh, A. B., Lim, H. N., & Tajudin, A. A. (2016). Electrochemical detection of uric acid via uricase-immobilized graphene oxide. *Analytical Biochemistry*, *509*, 135–141.

Wu, J., Liu, L., Cai, Y. R., & Yao, J. M. (2013). Recent advances of calcium phosphate nanoparticles for controlled drug delivery. *Mini-Reviews in Medicinal Chemistry*, *13*, 1501–1507.

Bharath, G., Madhu, R., Chen, S. M., Veeramani, V., Balamurugan, A., Mangalaraj, D., … Ponpandian, N. (2015). Enzymatic electrochemical glucose biosensors by mesoporous 1D hydroxyapatite on 2D reduced graphene oxide. *Journal of Materials Chemistry B*, *3*, 1360–1370.

Pang, P., Liu, Y., Zhang, Y., Gao, Y., & Hu, Q. (2014). Electrochemical determination of luteolin in peanut hulls using graphene and hydroxyapatite nanocomposite modified electrode. *Sensors & Actuators B: Chemical*, *194*, 397–403.

Wang, G., Shen, X., Yao, J., & Park, J. (2009). Graphene nanosheets for enhanced lithium storage in lithium ion batteries. *Carbon*, *47*, 2049–2053.

Guo, C. X., Yang, H. B., Sheng, Z. M., Lu, Z. S., Song, Q. L., & Li, C. M. (2010). Layered graphene/quantum dots for photovoltaic devices. *Angewandte Chemie International Edition*, *49*, 3014–3017.

Jia, X., Delgado, J. C., Terrones, M., Meunier, V., & Dresselhaus, M. S. (2011). Graphene edges: A review of their fabrication and characterization. *Nanoscale*, *3*, 86–95.

Teymourian, H., Salimi, A., Firoozi, S., Korani, A., & Soltanian, S. (2014). One-pot hydrothermal synthesis of zirconium dioxide nanoparticles decorated reduced graphene oxide composite as high performance electrochemical sensing and biosensing platform. *Electrochimica Acta*, *143*, 196–206.

Ghanbari, K. H., & Moloudi, M. (2016). Flower-like ZnO decorated polyaniline/reduced graphene oxide nanocomposites for simultaneous determination of dopamine and uric acid. *Analytical Biochemistry*, *512*, 91–102.

Zhou, M., Zhai, Y., & Dong, S. (2009). Electrochemical sensing and biosensing platform based on chemically reduced graphene oxide. *Analytical Chemistry*, *81*(14), 5603–5613.

He, C., Xie, M., Hong, F., Chai, X., Mi, H., Zhou, X., & Liu, J. (2016). A highly sensitive glucose biosensor based on gold nanoparticles/bovine serum albumin/Fe_3O_4 biocomposite nanoparticles. *Electrochimica Acta*, *222*, 1709–1715.

Masitas, R. A., Allen, S. L., & Zamborini, F. P. (2016). Size-dependent electrophoretic deposition of catalytic gold nanoparticles. *Journal of the American Chemical Society*, *138*(47), 15295–15298.

Li, R., Cai, Y., Yang, Y., Fang, S., Su, X., Sun, Y., & Yao, J. (2016). Dimensionally and morphologically controlled growth of calcium phosphate crystals by an organic-free hydrothermal process. *Ceramics International*, *42*, 17387–17397.

Li, X., Li, J., Liu, Y., Zhang, X., & Chen, J. (2017). A sensitive electrochemical immunosensor for prion detection based on poly-β-cyclodextrin/gold nanoparticles/glassy carbon electrode. *Sensors & Actuators B: Chemical*, *250*, 1–7.

Dey, R. S., & Raj, C. R. (2013). Redox-functionalized graphene oxide architecture for the development of amperometric biosensing platform. *ACS Applied Materials & Interfaces*, *5*, 4791–4798.

Kanyong, P., Pemberton, R. M., Jackson, S. K., & Hart, J. P. (2012). Development of a sandwich format, amperometric screen-printed uric acid biosensor for urine analysis. *Analytical Biochemistry*, *428*, 39–43.

Wang, X., Hu, C., Liu, H., Du, G., He, X., & Xi, Y. (2010). Synthesis of CuO nanostructures and their application for nonenzymatic glucose sensing. *Sensors & Actuators B: Chemical*, *144*, 220–225.

Rawal, R., Chawla, S., Chauhan, N., Dahiya, T., & Pundir, C. S. (2012). Construction of amperometric uric acid biosensor based on uricase immobilized on PBNPs/cMWCNT/PANI/Au composite. *International Journal of Biological Macromolecules*, *50*, 112–118.

Chauhan, N., & Pundir, C. S. (2011). An amperometric uric acid biosensor based on multiwalled carbon nanotube–gold nanoparticle composite. *Analytical Biochemistry*, *413*, 97–103.

How to cite this article: Chen Y, Zhou W, Ma J, Ruan F, Qi X, Cai Y. Potential of a sensitive uric acid biosensor fabricated using hydroxyapatite nanowire/reduced graphene oxide/gold nanoparticle. *Microsc Res Tech*. 2019;1–8. https://doi.org/10.1002/jemt.23410